Surface depression with double-angle geometry during the discharge of grains from a silo

F. Pacheco-Vázquez,* A. Y. Ramos-Reyes, and S. Hidalgo-Caballero
Instituto de Física, Benemérita Universidad Autónoma de Puebla, Apartado Postal J-48, Puebla 72570, Mexico
(Received 29 March 2017; revised manuscript received 25 June 2017; published 8 August 2017)

When rough grains in loose packing conditions are discharged from a silo, a conical depression with a single slope is formed at the surface. We observed that the increase of volume fraction generates a more complex depression, characterized by two angles of discharge: one at the bottom similar to the angle of repose and a considerably larger upper angle. The change in slope appears at the boundary between a dense stagnant region at the periphery and the central flowing channel formed over the aperture. Since the material in the latter zone is always fluidized, the flow rate is unaffected by the initial packing of the bed. On the other hand, the contrast between both angles is markedly smaller when smooth particles of the same size and density are used, which reveals that high packing fraction and friction must combine to produce the observed geometry. Our results show that the surface profile helps to identify by simple visual inspection the packing conditions of a granular bed, being useful to prevent undesirable collapses during silo discharge in industry.

DOI: 10.1103/PhysRevE.96.022901

I. INTRODUCTION

The discharge of dry grains from a container reveals several features of a granular material depending on the observation zone: If we look at the bottom, the discharged material accumulates, forming a conical heap, and the grains roll and slide in continuous or intermittent avalanches until the lateral face reaches the angle of repose θ_R [1]; if we look at the aperture, we observe a constant flow of grains Q independent of the height of the granular column [2], but we can also observe jamming if the opening is only a few times larger than the grain size [3,4]. Inside the container, on the other hand, the motion of the material towards the aperture can develop three different patterns: mass flow, funnel flow, or intermediate flow [5–8]. In the first case, typically observed in hoppers with very inclined walls, the material moves toward the outlet in a uniform manner, producing a continuous descent of the surface level; in the funnel flow, which is observed in silos with an opening through the horizontal bottom wall, an active flow channel forms above the outlet with stagnant material at the periphery; the third case of flow occurs when there is a combination of funnel flow in the lower part and mass flow in the higher part of the granular column. Flow pattern is fundamental to any understanding of stresses acting on the granular material, and modern techniques have been applied to visualize it, including particle image velocimetry, electrical capacitance tomography, and x-ray tomography [7–9]). Now, if we finally observe at the upper surface of the column, a conical depression may appear, with a slope slightly larger than the one corresponding to the maximum angle of stability θ_M, namely, the angle at which the material starts to flow [10,11].

Flow rate, flow patterns, and the angles θ_M and θ_R depend on different factors such as particle shape and size [12–14], rolling and sliding friction coefficients [15], roughness [16] wall separation [17], container and aperture size [2,18], polydispersity [19], volume fraction [9,20–22], and other complex parameters such as liquid content [23–25] and the acceleration of gravity [26,27]. It is well known that Q is mainly determined by the outlet-diameter-to-grain-size ratio and the kind of grains. Since the pioneering expression reported by Beverloo in that regard [2], more accurate models were lately proposed to include intermittent flow produced by jamming [4,18]. More recently, the discharge of granular materials has been investigated using submerged silos [28,29] or particles with repulsive magnetic interactions [30,31].

Although several investigations concerning silo discharge have been focused on the flow rate, the pile formation and the features of the flow pattern, the description of the upper depression, and its evolution during the discharge have gone unnoticed. Here, we report that, if a silo filled with sand is vibrated or tapped before the discharge, the flow rate is not affected by the increase of packing fraction but the surface depression suffers an important change in geometry. The most remarkable effect is the observation of two external angles that contrast with the constant slope of conical depressions typically reported in the literature for loose packing conditions [11,28,32]. The different dynamics can be appreciated in the snapshots shown in Fig. 1 and in a video in the Supplemental Material [33]. We found that the two surface angles appear because of the existence of two regions with distinct packing fractions: a peripheral stagnant zone and a less dense central zone flowing towards the aperture. Experiments in three-dimensional (3D) and two-dimensional (2D) silos were developed and the depression profile during the whole discharge was analyzed. On the other hand, a less pronounced change in slope was observed when spherical and smooth glass beads of the same size were used. This indicates that friction increases markedly due to the greater contact area among amorphous particles at high volume fractions, and such a combination produces the double-angle geometry.

II. EXPERIMENTAL SETUP

A. 3D system

A brass cylindrical container of 29 cm inner diameter and 30 cm height was used as a silo with a circular aperture of 0.65 ± 0.02 cm radius at the bottom face. The silo was filled

*fpacheco@ifuap.buap.mx

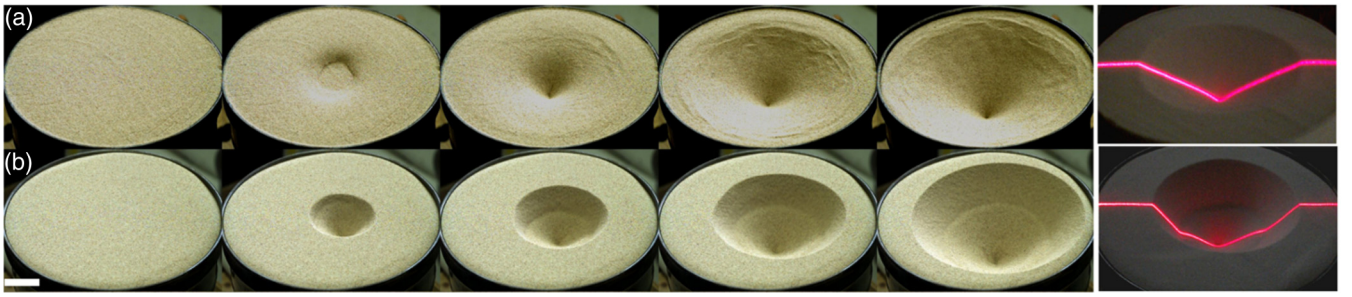

FIG. 1. Three-dimensional experiment: (a) Conical depression observed during the discharge of sand with loose packing fraction φ_l. (b) Depression with two surface angles observed when the same material is discharged with packing fraction $\varphi_p > \varphi_l$. In the last two snapshots, a laser line was used to better visualize the surface profile. The error bar corresponds to 5 cm.

with 31.5 kg of dry sand (density $\rho = 2.65 \pm 0.01$ g/cm^3 and size distribution of 150–250 μm). Then, the container was tapped laterally with a rubber hammer to increase the packing fraction. To measure the depression profile, a laser line was projected centrally on the sand surface during the discharge and it was recorded at 60 Hz with a lateral view at 45°. This procedure allowed us to observe the double-angle geometry as it is shown in Fig. 1(b).

B. 2D system

A quasi-two-dimensional cell was made of transparent glass walls of 0.5 cm thickness separated by an aluminum frame of inner dimensions $L = 28.00 \times H = 10.05 \times w = 0.31$ cm^3 and with a rectangular opening of 0.36×0.31 cm^2 centrally located at the bottom. The cell was filled with a mass $m = 136.4 \pm 0.1$ g of sand poured gently from the top to obtain a loose volume (packing) fraction $\varphi_l = m/LHw\rho \approx 0.59 \pm 0.01$. The cell was vertically located on a horizontal aluminum base mounted on two subwoofers controlled with a function generator which allowed us to apply a sinusoidal vibration of different voltage amplitudes V at a fixed frequency $f = 60$ Hz [see Fig. 2(a)]. With this frequency, the sand level decreased uniformly along the cell and the vibration was maintained until the sand surface reached a constant level H'. The larger the applied voltage, the larger was the shift in the sand level, revealing a higher volume fraction $\varphi_p = \varphi_l H/H'$ ranging in the interval $0.59 < \varphi_p < 0.68$. Figure 2(b) shows the dependence φ_p vs V fitted by the equation $\varphi_p = \varphi_l + \delta\varphi(1 - e^{-V/V_o})$, where $\varphi_l = 0.59 \pm 0.01$ is the loose packing obtained without vibration, $\delta\varphi = \varphi_{\max} - \varphi_l = 0.093$, and $V_0 = 42.4$ mV is the minimum voltage necessary to increase the packing of the bed. From the data fitting, we found the maximum packing fraction that can be reached with this granular material, $\varphi_{\max} = 0.685 \pm 0.005$. After the compaction process, the flow was started and the discharge was filmed at 125 fps with a high speed camera Photron SA3. The process was repeated five times for each value of ϕ and the videos were analyzed using IMAGEJ to measure the surface angles and total time of discharge. The main advantages of the 2D experiment are (i) a better control of packing conditions, and (ii) the possibility to observe the flow pattern during the whole discharge.

III. RESULTS

A. Surface profile and flow rate

Figures 2(c) and 2(d) show a comparison of two-dimensional discharges for a loose packing fraction $\varphi_l = 0.59 \pm 0.01$ and for a larger value $\varphi_p = 0.64 \pm 0.01$, respectively. As expected, a surface with a single angle $\theta = 37 \pm 1°$ in the first case is observed, but two angles appear when the packing fraction is increased. By illuminating the system from

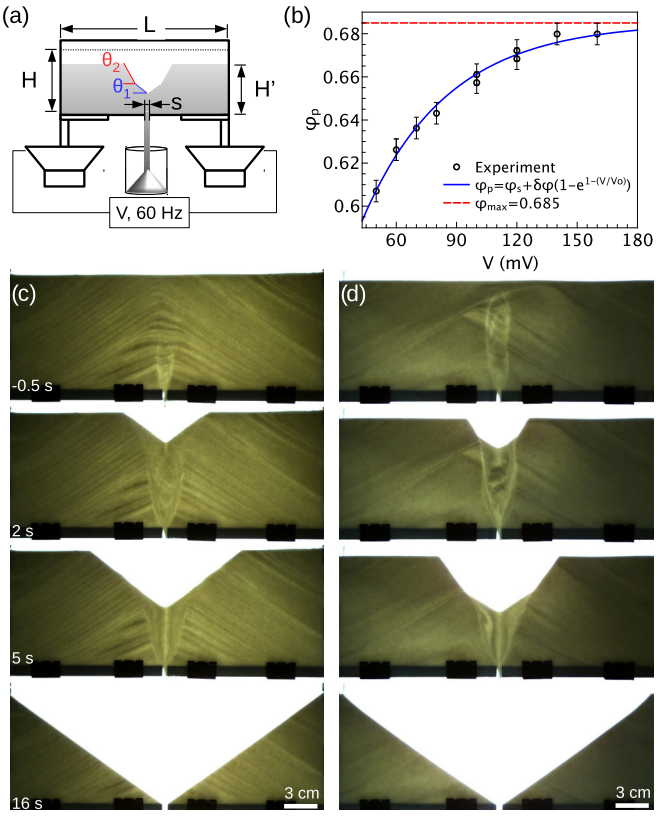

FIG. 2. Two-dimensional experiment: (a) Experimental setup; the surface angles θ_1 and θ_2 are indicated in the sketch. (b) Calibration curve indicating the packing fraction $\varphi_p = \varphi_l H/H'$ obtained when the cell is vibrated at different voltages V. Error bars are related to the standard deviation of the data. (c), (d) Snapshots of the discharge of sand with (c) loose packing $\varphi_l = 0.59$, and (d) higher packing $\varphi_p = 0.66$.

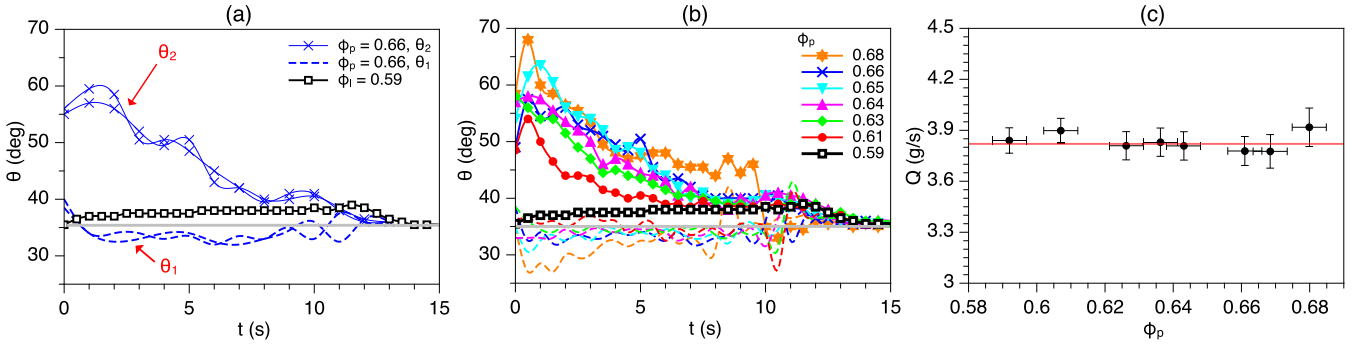

FIG. 3. Flow rate and time dependence of the two surface angles during the discharge: (a) θ vs t for $\varphi_l = 0.59$ (–□–) and $\varphi_p = 0.66$ [(–) θ_1; (×) θ_2]. (b) θ vs t for different values of φ_p. Lines with dots and dashed lines of the same color correspond to θ_2 and θ_1, respectively. The gray line indicates the angle of repose. The angle error due to image analysis was of the order of one pixel, corresponding to $\pm 1^\circ$. (c) The flow rate $Q = 3.82 \pm 0.05$ g/s is constant during the discharge and independent of the initial packing fraction of the bed (each point represents the average of five repetitions and error bars the standard deviation).

behind it is possible to observe the transition from a central zone where the material is flowing and the static lateral zones. The difference in packing produces a sharp contrast in light intensity which allows one to define clearly the funnel flow profile. Noteworthy, the transition coincides at the surface level with the point at which the slope changes, indicating an angle dependence on the volume fraction: The inferior angle θ_1 is related to a lower volume fraction in the fluidized zone and the upper angle θ_2 to the larger packing in the static zones. During the discharge, θ_2 decreases until it reaches the same value as θ_1 when the process ends.

Figures 3(a) and 3(b) show the values of θ_1 and θ_2 as a function of time t for different volume fractions φ_p. In the first plot only the cases $\varphi_l = 0.59$ and $\varphi_p = 0.66$ are compared for clarity. Two repetitions exemplify the reproducibility of the process observed in all the events. For the loose packing case (□), the slope fluctuates around the angle of stability $\theta \approx 37.5^\circ$ and then falls at the end of the discharge to $\theta_R = 35.5^\circ$ (gray line), the angle of repose for this granular material. On the other hand, for the highly packed bed, θ_2 (×) reaches up to 60° at the beginning of the discharge while θ_1 (–) falls below the angle of repose, and then both angles converge at the end of the process in $\theta = \theta_R$. In general, the same dynamics is observed for different values of $\varphi_p > \varphi_l$ [see Fig. 3(b)]: θ_2 increases with φ_p (line+symbol) while θ_1 decreases (dashed lines), and always $\theta_1 < \theta_R < \theta_2$. Note that in all cases the discharge finishes practically at the same time τ. Accordingly, Fig. 3(c) shows that the flow rate $Q = \Delta m/\Delta t$ (where Δm is the mass of grains discharged during a time Δt) measured through the aperture for different values of φ_p is constant. Equivalent measurements in the 3D case give $Q = 63.7 \pm 0.9$ g/s for loose packing ($\varphi_l \approx 0.60 \pm 0.01$) and $Q = 64.8 \pm 0.7$ g/s for high packing ($\varphi_p \approx 0.64 \pm 0.01$). Therefore, Q is independent of the initial packing of the bed in both 2D and 3D systems.

Figure 4(a) shows the radius of the 2D depression R_{2D} as a function of time for different values of φ_p. The log-log plot in the inset reveals a nearly linear relation indicating a power-law dependence $R(t) = C(\varphi_p)t^{n(\varphi_p)}$. The maximum growth rate is observed for the loose packing case (□), and the best fit of the data gives $R(t)_{2D} = (3.32 \pm 0.02)t^{0.521\pm0.003}$ (black line). For higher packing values, the radius grows more slowly over time and is well fitted by a power law with coefficients $C(\varphi_p)$ and exponents n whose dependence on φ_p is derived in the following section. Figure 4(b) shows a similar dynamics for the 3D case, with the best fit given by $R(t)_{3D} = (3.59 \pm 0.01)t^{0.333\pm0.005}$ (black line) for φ_l, and a slower cavity growth for φ_p (red line). It can be also notice that R_{3D} has stepwise increments for $t > 20$ s in the latter case, in contrast to the smooth increase of R_{3D} for loose packing. Videos reveal that this is due to abrupt avalanches of material produced at large values of θ_2, when the surface becomes unstable at one point where the weight of the material above it surpasses friction.

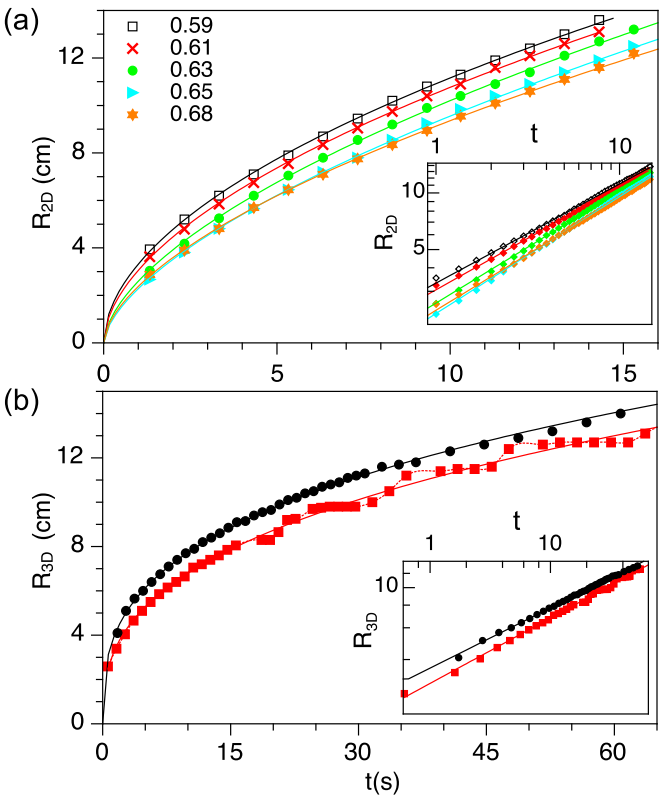

FIG. 4. Cavity radius as a function of time for (a) 2D and (b) 3D discharges of loosely (black dots) and densely (red squares) packed grains. Insets: Corresponding log-log plots indicate a nearly-power-law growth.

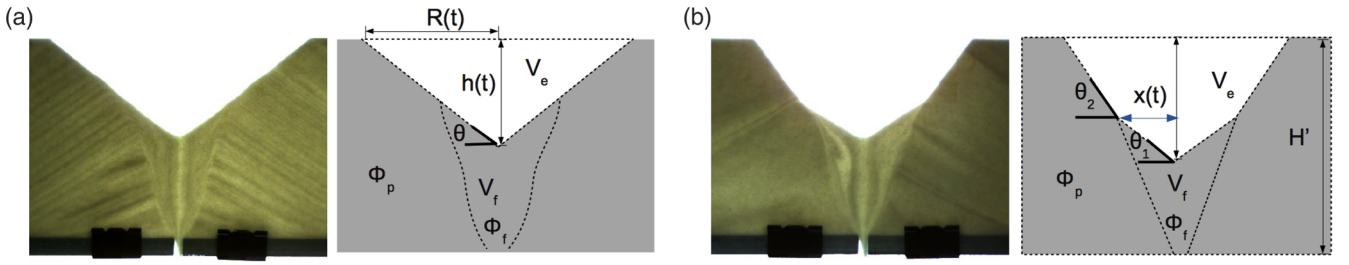

FIG. 5. Snapshots and diagrams showing the geometry of the cavity for (a) loosely and (b) previously packed systems. V_e indicates the empty volume and V_f the volume occupied by the fluidized material.

B. Geometrical model

Let us now obtain a general expression for $R(t)$ and then consider each particular case (2D, 3D, and loosely or highly packed bed). Let φ_p and φ_f be the volume fractions of the static lateral zones and the fluidized central zone, respectively. From Fig. 5, the volumes of the empty depression V_e and the fluidized zone V_f were initially occupied by a mass of grains $\rho\varphi_p(V_e + V_f)$; this mass must be equal at a given time t to the discharged mass Qt plus the remaining fluidized grains in V_f with volume fraction φ_f; therefore, one can write $\rho\varphi_p(V_e + V_f) = Qt + \rho\varphi_f V_f$. Hence we get

$$\varphi_p V_e + (\varphi_p - \varphi_f)V_f = \rho^{-1} Qt. \tag{1}$$

When the material is discharged in loose packing conditions, the difference between θ_1 and θ_2 is negligible and we can assume $\varphi_p = \varphi_l \approx \varphi_f$; thus, the second term in Eq. (1) vanishes and V_e in 2D is approximately the volume of the triangular depression indicated in the scheme of Fig. 5(a); then, $\varphi_l Rhw = \rho^{-1} Qt$, where w is the cell width. Since $h = R\tan\theta$, we simply obtain

$$R(t)_{2D} = Ct^{0.5}, \quad C = \sqrt{\frac{Q}{\rho\varphi_l w \tan\theta}}. \tag{2}$$

Using the experimental parameters, one gets $C = 3.23 \pm 0.09\,\mathrm{cm/s^{1/2}}$. This value and the exponent $n = 0.5$ obtained from the analysis are in excellent agreement with the best fit of the data shown in Fig. 4(a) for the loose volume fraction. The small difference in exponents can be understood considering that φ_f is actually slightly smaller than φ_l.

On the other hand, the solution of Eq. (1) for larger volume fractions demands an expression for V_e and V_f; if $x(t)$ is the x coordinate of the transition point [see the scheme in Fig. 5(b)], we can approach the volumes $V_e = x^2 w(\tan\theta_1 - \tan\theta_2) + R^2 w\tan\theta_2$, and $V_f = w(H' - R\tan\theta_2)x + x^2 w(\tan\theta_2 - \tan\theta_1)$, where R, x, θ_1, and θ_2 depend on time; then, Eq. (1) can be written as $\varphi_p R^2\tan\theta_2 + (\varphi_p - \varphi_f)(H\varphi_f/\varphi_p - R\tan\theta_2)x + \varphi_f x^2(\tan\theta_1 - \tan\theta_2) = \rho^{-1}w^{-1}Qt$, which is a quadratic equation in $R(t)$ with a general solution

$$R(t)_{2D} = -\frac{x}{2}\left(1 - \frac{\varphi_f}{\varphi_p}\right) \pm \left\{\left[\frac{1}{4}\left(1 - \frac{\varphi_f}{\varphi_p}\right)^2 + \left(1 - \frac{\tan\theta_1}{\tan\theta_2}\right)\frac{\varphi_f}{\varphi_p}\right]x^2 + \frac{Qt}{\rho\varphi_p w\tan\theta_2}\right\}^{0.5}. \tag{3}$$

Note that Eq. (3) reduces to Eq. (2) for the conical case, where $\varphi_f, \varphi_p \approx \varphi_l$ and $\theta_1 = \theta_2$. To obtain a numerical solution of Eq. (3), we can assume based on Fig. 3(b) that $\theta_1 \approx \theta_R$ and a hyperbolic dependence for $\theta_2 = \theta_0/(1 + \beta t)$, where θ_0 is the maximum angle at the beginning of the discharge and $\beta = (\theta_0/\theta_R - 1)/\tau$. Moreover, we used a parabolic dependence for $x(t)$ according to measurements of the funnel flow profile shown in the inset of Fig. 6(a). Under such considerations, one obtains that the positive solutions for $R_{2D}(t)$ ploted in $\log_{10} - \log_{10}$ in Fig. 6(a) for different packing fractions (dashed lines) are in very good agreement with experiments (points). The log-log plot shows that the numerical solutions

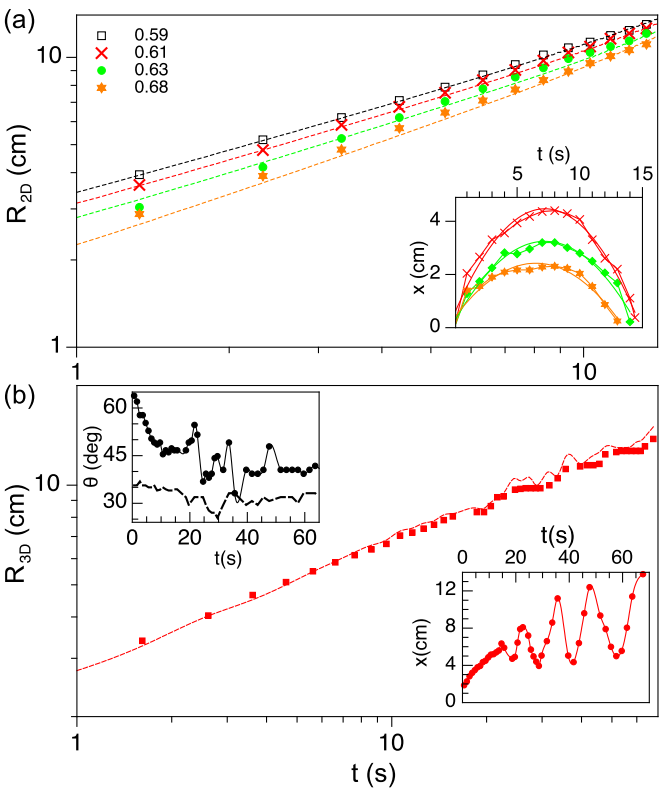

FIG. 6. Log-log plots of R vs t for (a) 2D and (b) 3D discharges obtained from the solution of Eqs. (3) and (5), respectively. In (a), solutions for different values of φ_p (dashed lines) are compared with experiments (points). The insets on the right show the transition coordinate x vs t obtained from a video analysis in each case. In (b), the inset on the left shows θ_1 and θ_2 vs t during a 3D discharge with $\varphi_p = 0.64$.

predict the slight deviation from a power law observed in the experimental data.

Regarding the 3D case, Eq. (1) remains valid with a depression described by a conical shape of volume $V_e = \frac{1}{3}\pi R^2 h$ for the discharge of loosely packed material. Considering again $\varphi_f \approx \varphi_l$ and $h = R\tan\theta$ for this trivial case, one obtains

$$R(t)_{3D} = C' t^{1/3}, \quad C' = \left(\frac{3Q}{\rho\varphi_l \pi \tan\theta}\right)^{1/3}. \tag{4}$$

Using the experimental values one finds $C' = 3.67 \pm 0.05\,\mathrm{cm/s^{1/3}}$, again in very good agreement with the 3D data fitting reported above. As in the 2D analysis, an expression for larger φ_p can be derived based on Fig. 5(b). In this case, Eq. (1) can be written as $\varphi_p \tan\theta_2 R^3 + \varphi_f x^3(\tan\theta_1 - \tan\theta_2) + (\varphi_p - \varphi_f)x^2(H\varphi_f/\varphi_p - R\tan\theta_2) = 3Qt/\pi\rho$. The third term of the left-hand side is one order of magnitude smaller than the others, therefore, one finds

$$R(t)_{3D} \approx \left[\frac{3Qt}{\rho\varphi_p\pi\tan\theta_2} + \frac{\varphi_f}{\varphi_p}\left(1 - \frac{\tan\theta_1}{\tan\theta_2}\right)x^3\right]^{1/3}. \tag{5}$$

As it is to be expected, the latter expression is reduced to Eq. (4) when $\theta_1 = \theta_2$. To solve Eq. (5) for the packed case ($\varphi_p = 0.64$), we measured θ_1, θ_2, and x as a function of t using laser profilometry. The resulting data shown in the insets of Fig. 6(b) reveal a very complex dependence on time after $t = 20$ s, related to abrupt avalanches of sliding material. It is worth mentioning that the avalanches appear periodically, as in the stick slip motion of granular layers. We must also consider that the tapping compaction method could produce a nonhomogeneous packing inside the 3D silo, which generates large fluctuations in the values of θ_2. Since it was not feasible to establish analytical expressions for x and θ_2, data were substituted directly in Eq. (5), and one gets a very good agreement between the solution (–) and the experiment (■) in Fig. 6(b). Thus, $R(t)$ is well described by one-half and one-third power laws with dependence on de packing fraction given by Eqs. (3) and (5) for 2D and 3D discharges, respectively.

C. Rough grains versus smooth grains

Although a high volume fraction seems to be necessary to obtain two angles of discharge, smooth spherical glass particles discharged from the 2D silo apparently develop only one surface angle independently of φ_p [see Fig. 7(a)]. A thorough analysis of the packed case ($\varphi_p = 0.64$) at the transition zone reveals a slope difference $\theta_2 - \theta_1 \approx 4^\circ$ [see Fig. 7(b)]. This is a small change compared to the difference of up to 30° observed during the discharge of sand grains for the same packing conditions. Glass beads used in the experiments have approximately the same density ($\rho \approx 2.65 \pm 0.02$ g/cm^3) and average size ($d \approx 200$ μm) than sand grains; the main difference between them is the particle shape and roughness, as it can be noticed from images taken with a microscope [see Fig. 7(c)]. In addition, two consecutive snapshots of the videos were subtracted to visualize the flowing grain layer [see Figs. 7(d) and 7(e)]. The treatment reveals that the glass bead layer is almost twice thicker than the sand layer, while they are approximately of the same thickness in loose packing conditions. Another visible difference is the sudden transition from the moving sand layer to the static zone, which exhibits

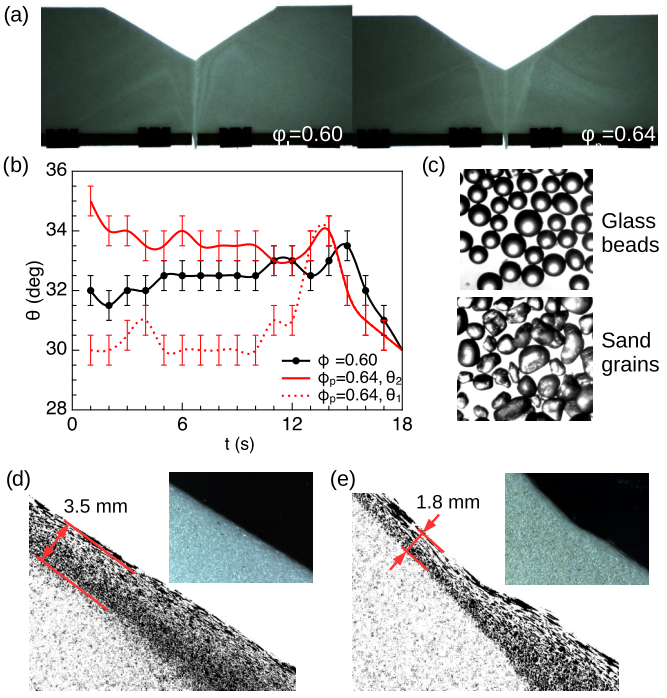

FIG. 7. (a) Discharge of the 2D cell with glass beads for $\varphi_l = 0.60$ and $\varphi_p = 0.64$. (b) Surface angles as a function of t during the discharge of glass beads. (c) Photos taken with a microscope used to compare the grain morphology. (d), (e) Closeup view of the flowing layer of glass beads and sand grains, respectively. The approximate thickness of the moving layer is indicated.

a greater shear resistance of this material. Then, the particle geometry and roughness are important factors that determine the surface dynamics. Nonetheless, regardless the packing fraction of the bed, the flow rate measured with glass beads was $Q = 3.86 \pm 0.04$ g/s, approximately the same value obtained with sand grains.

IV. DISCUSSION AND CONCLUSIONS

According to our observations, the surface profile can be useful to determine the packing conditions of the granular bed. For a loose volume fraction, the difference between the maximum angle of stability in the static zone and in the fluidized zone is small and it cannot be distinguished at a glance, but a larger contrast between these angles is a clear indication of a highly packed material. Moreover, the greatest change is observed with rough amorphous grains, and this scenario is the most common and closest to large-scale processes if we consider that edible grains in agriculture, cement, gravel, and other materials in industry are indeed rough nonspherical particles. The results presented here are in agreement with previous studies about the stability of heaps made of natural granular materials [12], where it was found that less spherical particles have greater stability angles. Similar results were obtained using rotating drum systems, showing an important increase of θ_m in two-dimensional heaps of trapezoids and diamond-shaped grains compared to more rounded geometries [14,20]. It was also found in the last reference that for most of the geometries the heap stability

increases with packing fraction, which is also consistent with our findings.

Two external angles of stability have also been recently reported in numerical investigations of very large three-dimensional heaps of particles produced by ballistic deposition [34]. In that research, it was found that distinct density zones produced during the deposition have a remarkable implication in the angle of repose, and the angle change was associated with an increase in the number of contacts among beads. This coincides with our explanation of the notable increase of angle for nonspherical particles: Amorphous grains can be rearranged under vibration to maximize the contact area, in contrast to glass beads whose contact is reduced to a surface point; therefore, a grain of sand experiences more friction with the surrounding particles and needs on average a greater angle of inclination to start moving.

Another aspect to notice is that the relation $\theta_1 < \theta_R < \theta_2$ is always satisfied. Since θ_1 is the angle corresponding to the fluidized zone with volume fraction φ_f, its value should be independent on φ_p; nevertheless, θ_1 slightly decreases when the initial packing of the bed is augmented. To explain this fact, let us remember that the fluidized zone is fed by the thin layers of grains flowing over the static zones. Considering an average friction coefficient μ, these grains have an acceleration $a \sim g(\sin\theta_2 - \mu\cos\theta_2)$, where g is the acceleration of gravity. Thus, the velocity at which they arrive to the fluidized zone is greater for higher values of θ_2 and they can move further to be accumulated near the central zone. The accumulation of particles generates a slope with $\theta_1 < \theta_R$ and it allows the avalanche to stop. Furthermore, in Fig. 3 we showed that θ_2 decreases over time. This is also related to the accumulation of grains in the central zone and only happens if the flow from the lateral zones is greater than the flow through the outlet. As the discharge time t increases, the distance from the cavity rim to the fluidized zone augments and the upper angle must diminish from geometrical requirements. Thus, θ_2 would not change if such a distance were constant. To test this point, we performed experiments in a tall cell with $H > (L/2)\tan\theta_R$ [see Fig. 8(a)]. By comparing the snapshots with the analysis shown in Fig. 8(b) we can notice that indeed θ_2 remains constant during a considerable part of the discharge (stage II) because the length of the flowing layer over the stagnant zone is practically the same in such an interval. The same dynamics was observed in an even larger silo [Fig. 8(c)] and in all cases a funnel flow is developed.

It is interesting to note that the loose packing fraction φ_l handled here coincides with the critical packing value ($\varphi_{cps} \sim 0.59$) reported in Refs. [35,36] for which density fluctuations are minimized, and shear does not cause either dilation or compaction of the granular bed. This supports our assumption about the negligible difference in volume fraction between flowing and stagnant regions for this packing value, and it helps to clarify why there are no changes in the surface slope or sudden avalanches, as it occurs for higher packing values.

Finally, let us argue about the independence of Q on the volume fraction shown in Fig. 3(c). This can be understood if we observe from snapshots in Figs. 2(c) and 2(d) that the material from the stagnant zone must pass through the fluidized zone before reaching the aperture; therefore, the initial volume

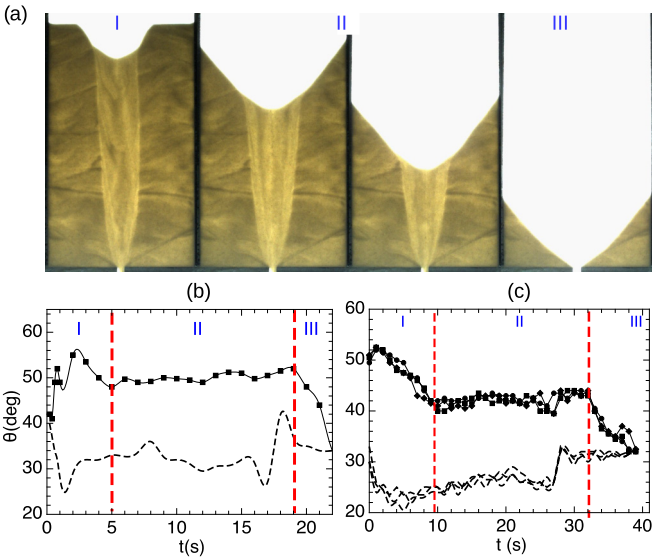

FIG. 8. (a) Snapshots of the discharge of a 2D tall silo. (b) θ_1 and θ_2 as a function of t. Three regimes are observed and each one ends when (I) the cavity reaches the side walls, (II) the cavity reaches the outlet, and (III) the flow stops at the angle of repose. In (II) the surface angles remain almost constant. (c) θ_1 and θ_2 vs t in a considerably larger quasi-2D silo filled with 1.5 kg of sand.

fraction of the bed is irrelevant. To support our conclusion, we plot in Fig. 9(a) the velocity field in the x-z plane obtained from particle trajectories tracked in the fluidized zone during the discharge of loose and packed beds. In Figs. 9(b) and 9(c) we can notice that the velocity values v are very similar for both packings, with a maximum in $(x,z) \sim (0,10)$, i.e., in the

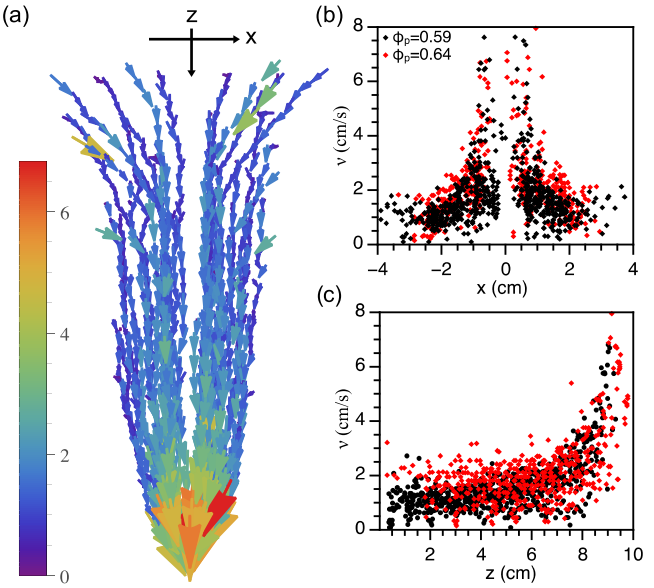

FIG. 9. (a) Velocity field obtained from particle tracking during the discharge of loosely and highly packed grains. (b) v as a function of the x coordinate. (c) v at different z coordinates. The velocity is almost constant along the funnel and increases abruptly near the outlet.

outlet, and it decreases symmetrically as we move away from the central zone. The notable increase of v when the material passes through the outlet is because the funnel flow suddenly narrows and it must obey mass conservation. In this lower point, the grains reach similar speeds in both discharges ($v \approx 8$ cm/s), which explains the constant flow rate independently of the initial packing of the bed. In the literature, even though the flow rate in vertical silos filled under different conditions has been investigated [37], small flow-rate variations were related to changes in pressure and not to the packing fraction itself, and little effect on the flow was expected in vertical silos packed by the influence of gravity [22]. A dependence of Q on the value of φ only was found to be important in vertical [38] and horizontal silos [22] in a regime of dilute flows of particles, where a higher concentration at the outlet produces a larger amount of grains leaving the system. Then, it could be of interest for future research to explore the flow-rate transition from dilute to dense flows of granular materials.

In summary, this research shows that the depression profile during the discharge of grains from a silo develops a richer dynamics if the material is previously compacted. The time dependence of the depression radius in 2D and 3D silos follows respectively one-half and one-third power laws that are functions of the packing fraction. In all cases, the flow rate is independent of the initial packing of the bed because the grains enter in a fluidized zone before reaching the silo aperture. The observation of two angles in the surface profile is clear indication of a highly packed material, and it can help to prevent abrupt avalanches that could produce silo damage.

ACKNOWLEDGMENTS

This research was supported by the following projects: CONACyT Mexico No. 242085 of the Sectoral Research Fund for Education, PRODEP-SEP No. DSA/103.5/14/10819, PROFOCIE-SEP 2015-2016, and VIEP 2016-2017.

[1] J. Duran, *Sands, Powders, and Grains: An Introduction to the Physics of Granular Materials* (Springer, New York, 2000).
[2] W. A. Beverloo, H. A. Leniger, and J. van de Velde, Chem. Eng. Sci. **15**, 260 (1961).
[3] I. Zuriguel, A. Garcimartín, D. Maza, L. A. Pugnaloni, and J. M. Pastor, Phys. Rev. E **71**, 051303 (2005).
[4] I. Zuriguel *et al.*, Sci. Rep. **4**, 7324 (2014).
[5] T. V. Nguyen, C. E. Brennen, and R. H. Sabersky, J. Appl. Mech. **47**, 729 (1980).
[6] A. Drescher, Powder Technol. **73**, 251 (1992).
[7] J. Tejchman, *Confined Granular Flow in Silos: Experimental and Numerical Investigations* (Springer, Berlin, 2013).
[8] K. Grudzien, Image Process. Commun. **19**, 107 (2015).
[9] L. Babout, K. Grudzien, E. Maire, and P. J. Withers, Chem. Eng. Sci. **97**, 210 (2013).
[10] R. Albert, I. Albert, D. Hornbaker, P. Schiffer, and A.-L. Barabasi, Phys. Rev. E **56**, R6271(R) (1997).
[11] G. Boumans, *Grain Handling and Storage* (Elsevier, Amsterdam, 2012).
[12] P. A. Arias-García, R. O. Uñac, A. M. Vidales, and A. Lizcano, Physica A **390**, 4095 (2011).
[13] D. A. Robinson and S. P. Friedman, Physica A **311**, 97 (2002).
[14] C. J. Olson, C. Reichhardt, M. McCloskey, and R. J. Zieve, Europhys. Lett. **57**, 904 (2002).
[15] Y. C. Zhou, B. H. Xu, A. B. Yu, and P. Zulli, Powder Technol. **125**, 45 (2002).
[16] N. A. Pohlman, B. L. Severson, J. M. Ottino, and R. M. Lueptow, Phys. Rev. E **73**, 031304 (2006).
[17] S. Courrech du Pont, P. Gondret, B. Perrin, and M. Rabaud, Europhys. Lett. **61**, 492 (2003).
[18] C. Mankoc *et al.*, Granular Matter **9**, 407 (2007).
[19] L. Pournin, M. Ramaioli, P. Folly, and Th. M. Liebling, Eur. Phys. J. E **23**, 229 (2007).
[20] J. Olson, M. Priester, J. Luo, S. Chopra, and R. J. Zieve, Phys. Rev. E **72**, 031302 (2005).
[21] R. O. Uñaca, A. M. Vidales, and L. A. Pugnaloni, J. Stat. Mech. (2012) P04008.
[22] M. A. Aguirre, R. De Schant, and J.-C. Geminard, Phys. Rev. E **90**, 012203 (2014).
[23] S. Nowak, A. Samadani, and A. Kudrolli, Nat. Phys. **1**, 50 (2005).
[24] M. Scheel *et al.*, Nat. Mater. **7**, 189 (2008).
[25] F. Pacheco-Vázquez, F. Moreau, N. Vandewalle, and S. Dorbolo, Phys. Rev. E **86**, 051303 (2012).
[26] M. G. Kleinhans, H. Markies, S. J. de Vet, A. C. in 't Veld, and F. N. Postema, J. Geophys. Res. **116**, E11004 (2011).
[27] S. Dorbolo *et al.*, Granular Matter **15**, 263 (2013).
[28] T. Wilson, C. Pfeifer, N. Mesyngier, and D. Durian, Pap. Phys. **6**, 060009 (2014).
[29] J. Koivisto and D. J. Durian, Nat. Commun. **8**, 15551 (2017).
[30] G. Lumay *et al.*, Pap. Phys. **7**, 070013 (2015).
[31] D. Hernández-Enríquez, G. Lumay, and F. Pacheco-Vázquez, EPJ Web Conf. **140**, 03089 (2017).
[32] F. E. Loranca-Ramos, J. L. Carrillo-Estrada, and F. Pacheco-Vázquez, Phys. Rev. Lett. **115**, 028001 (2015).
[33] See Supplemental Material at http://link.aps.org/supplemental/10.1103/PhysRevE.96.022901 for the discharge of loosely and highly packed grains from three dimensional and two dimensional systems. Note the appearance of two angles of discharge on the surface of the highly packed bed.
[34] N. Topić, J. A. C. Gallas, and T. Pöschel, Phys. Rev. Lett. **109**, 128001 (2012).
[35] M. Schröter, D. I. Goldman, and H. L. Swinney, Phys. Rev. E **71**, 030301(R) (2005)
[36] P. Umbanhowar and D. I. Goldman, Phys. Rev. E **82**, 010301(R) (2010).
[37] H. Ahn, Z. Başaranoğlu, M. Yilmaz, A. Buğutekin, and M. Zafer Gül, Powder Technol. **186**, 65 (2008).
[38] D. Huang, G. Sun, and K. Lu, Phys. Rev. E **74**, 061306 (2006).